NMR Imaging and Hydrodynamic Analysis of Neutrally Buoyant Non-Newtonian Slurry Flows

by
J. X. Bouillard
Argonne National Laboratory
9700 S. Cass Avenue
Argonne, IL 60439
and
S. W. Sinton
Lockheed Missiles and Space Co.
Lockheed Palo Alto, Research Laboratory
Palo Alto, California 94304

Introduction

The flow of solids loaded suspension in cylindrical pipes has been the object of intense experimental and theoretical investigations in recent years. These types of flows are of great interest in chemical engineering because of their important use in many industrial manufacturing processes. Such flows are for example encountered in the manufacture of solid-rocket propellants, advanced ceramics, reinforced polymer composites, in heterogenous catalytic reactors, and in the pipeline transport of liquid-solids suspensions. Similar slurry processes as for example those using paper pulp and tomato juices are frequently encountered in the Food and Paper industries. In most cases, the suspension microstructure and the degree of solids dispersion greatly affect the final performance of the manufactured product. For example, solid propellant pellets need to be extremely-well dispersed in gel matrices for use as rocket engine solid fuels. The homogeneity of pellet dispersion is critical to allow good uniformity of the burn rate, which in turn affects the final mechanical performance of the engine. Today's manufacturing of such fuels uses continuous flow processes rather than batch processes. Unfortunately, the hydrodynamics of such flow processes is poorly understood and is difficult to assess because it requires the simultaneous measurements of liquid/solids phase velocities and volume fractions. Commonly used non-invasive flow measurements are usually based on light (laser doppler anenometry), sound waves, X/

DISCLAIMER

gamma ray, particle beam or electrical impedance techniques which all suffer from attenuation, opacity and scattering across immiscible phase interfaces, especially at high solids loadings.

In contrast, Nuclear Magnetic Resonance (NMR) techniques usually do not experience transmission effects in nonconducting media and are truly non-invasive. NMR imaging presents the potential to non-invasively determine hydrodynamic parameters of complex flow processes such as solids/liquid volume fractions and multiple phase flow velocities [1, 2, 3, 4, 5, 6].

Due to the recent development in pulsed Fourier Transform NMR imaging, NMR imaging is now becoming a powerful technique for the non intrusive investigation of multi-phase flows. Kose et al. [7] originally introduced two-dimensional NMR flow imaging techniques which result in both velocity profiles and flow compensated liquid volume fraction distributions. Later, Majors et al. [1] used this technique to measure slurry flows of up to 2 m /sec. These latter investigators further argue that turbulence measurement could even be possible in principle. It is however prudent to first expose and discuss the recently developed experimental and theoretical techniques to study simple laminar neutrally buoyant non-Newtonian flows. This paper is a first step in this direction, for it reports and exposes a state-of-the-art experimental and theoretical methodologies that can be used to study such flows. The hydrodynamic model developed for this study is a two-phase flow shear thinning model with standard constitutive fluid/solids interphase drag and solids compaction stresses. This model shows good agreement with experimental data and the limitations of this model are discussed.

Hydrodynamic Flow Models

A transient pilot-scale two-dimensional two-phase flow computer program written in cartesian and cylindrical coordinates specifically developed to study liquid-solids slurry flow was used to analyze the NMR flow data. The hydrodynamic computer model is presented in Table 1. As can be seen, the carrier phase is treated as a Newtonian fluid, whereas the suspended solids phase is treated as a non-Newtonian medium. A phenomenological shear-thinning formulation was adopted with the standard fluid/solids interphase friction and solids compaction stress constitutive equations to describe the

Table 1: Governing Hydrodynamic Equations

Continuity and Momentum Equations

$\partial(\epsilon_l \rho_l)/\partial t + \nabla.(\rho_l \epsilon_l v_l) = 0$

$\partial(\epsilon_s \rho_s)/\partial t + \nabla.(\rho_s \epsilon_s v_s) = 0$

$\partial(\epsilon_l \rho_l v_l)/\partial t + \nabla.(\rho_l \epsilon_l v_l v_l) = -\nabla P + \epsilon_l \rho_l g + \beta(v_s - v_l) - \nabla.(\epsilon_l \tau_l)$

$\partial(\epsilon_s \rho_s v_s)/\partial t + \nabla.(\rho_s \epsilon_s v_s v_s) = -\nabla.(\epsilon_s \tau_s + \tau_c) + \epsilon_s \rho_s g + \beta(v_l - v_s)$

Constitutive Equations

Inter-Phase Coefficient β

$\epsilon_l \leq 0.8 \qquad \beta = 150\frac{(1-\epsilon_l)^2 \mu_l}{\epsilon^2 (d_p \phi_s)^2} + 1.75\frac{\rho_l |v_l - v_s|(1-\epsilon_l)}{(\epsilon d_p \phi_s)}$

$\epsilon_l > 0.8 \qquad \beta = \frac{3}{4} Cd \frac{|v_l - v_s| \rho_l (1-\epsilon_l)}{\epsilon_l d_p \phi_s} \epsilon_l^{-2.65}$

with:

$Cd = \frac{24}{Re}(1 + 0.15 Re^{0.687}) \qquad Re \leq 1000$

$Cd = 0.44 \qquad Re > 1000$

$Re = \frac{|v_l - v_s| d_p \rho_l \epsilon_l}{\mu_l}$

Phase Viscous Stresses

$\tau_k = -\mu_k(\nabla v_k + (\nabla v_k)^T)$

Solids Compaction Stresses

$\nabla \tau_c = G(\epsilon_s) \nabla \epsilon_s$

with

$G(\epsilon_s) = exp(-500(\epsilon_l - 0.43))$

rheology of the slurry [8, 9, 10, 11].

In the equation of motion described in Table 1, an interphase drag coefficient, β, between the liquid and solids phases is used as constitutive equation. Discussion regarding the modeling of this term may be found in [8, 9]. These same papers discussed the modeling of the solids compaction stress τ_c. The shear stress required for the solids phase, τ_s, is formulated by considering that the total solids/liquid mixture behaves as a non-Newtonian fluid, exhibiting a power law shear thinning characteristic. The phenomenological equations adopted in this study to describe the mixture rheology can be symbolically written as:

$$\tau_{mix} = \epsilon_l \tau_l + \epsilon_s \tau_s = -K(\epsilon_s)(\nabla v_{mix} + (\nabla v_{mix})^T)^{n(\epsilon_s)} \tag{1}$$

where

$$\tau_l = -\mu_l(\nabla v_l + (\nabla v_l)^T) \tag{2}$$

The mixture shear stress can be expressed as function of a mixture viscosity μ_{mix} as

$$\tau_{mix} = -\mu_{mix}(\nabla v_{mix} + (\nabla v_{mix})^T)^{n-1} \tag{3}$$

where the mixture velocity is defined as:

$$v_{mix} = (\epsilon_s \rho_s v_s + \epsilon_l \rho_l v_l)/(\epsilon_l \rho_l + \epsilon_s \rho_s)$$

The values of $K(\epsilon_s)$, the consistency index, and $n(\epsilon_s)$, the power-law index, are mixture dependent and have to be measured experimentally. Such an approach has been successively used by Lyczkoski and Wang [12] In our study, the mixture viscosity was experimentally measured using a Couette cell as a function of the solids concentration and the mixture shear rate. As can be seen in Figure 1, the mixture viscosity exhibits a strong dependence upon the solids volumetric concentration, exhibiting an exponential dependency. It is only at high solids concentrations that a shear thinning behavior can be observed as indicated in this figure.

For the solids/liquid system considered in this study, Basset forces [13], slip-shear lift forces [14, 15], Magnus forces [16], and virtual mass forces [17, 18] have been neglected. Because of the small particle diameter and the large viscosity of the carrier fluid, an order of magnitude analysis indicated

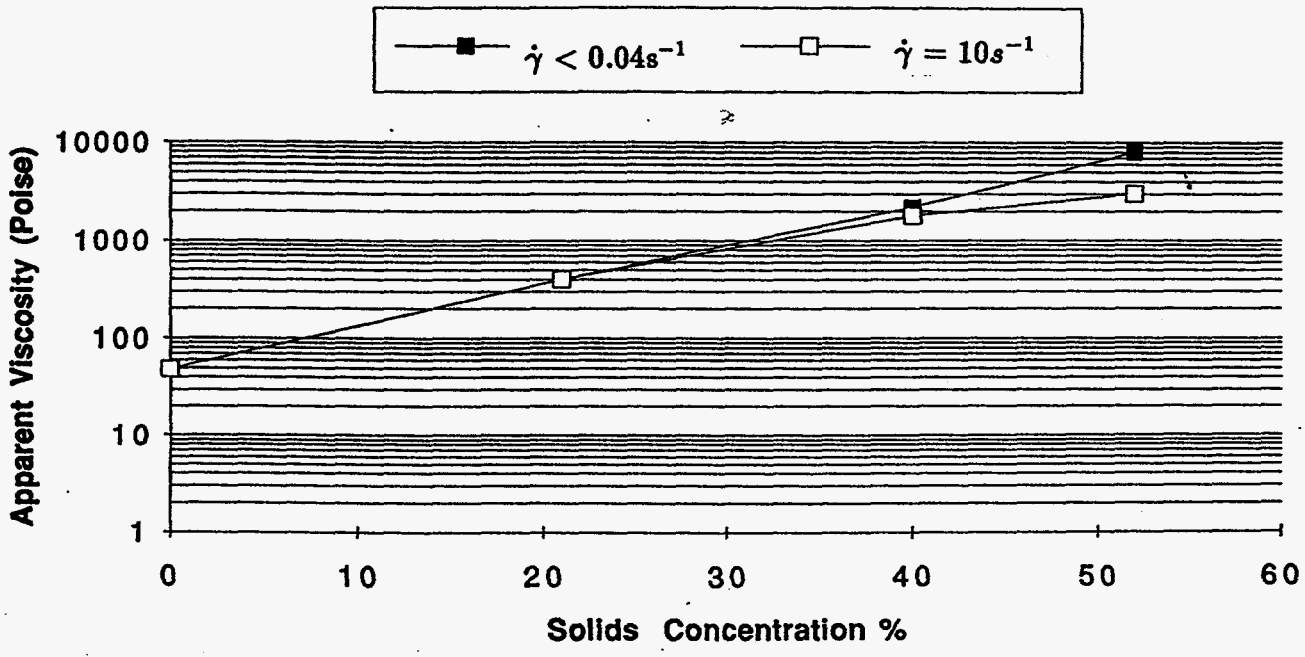

Figure 1: Experimentally Measured Mixture Viscosity Dependency upon Solids Concentration and Shear Rates

that all these forces are small when compared to the interphase drag forces. Added mass forces depend on relative acceleration between solids and liquid phases, and thus become vanishingly small for fully developed flows. Since it is anticipated that the solid particles move about the same velocity as the fluid, a zero velocity boundary condition is imposed for both phases at the wall of the pipe.

Experimental Methodology

A time of flight spin echo sequence, as presented in Figures 2 and 3, was used to measure the the liquid velocity. The basic method was developed by Kose et al. [7] and later extended by Majors et al. [1]. Application of a selective RF pulse at the same time as a gradient at the start of the sequence excites a slice of magnetized protons of the carrier fluid in the stream. The slice is perpendicular to the flow direction Oz and the thickness size is determined by the RF bandwidth and gradient strength. Slice excitation is followed by two broadband π pulses which have the effect of refocusing the phases of different isochromats in the sample. At 4 τ, a selective echo is detected as shown in Figure 2 [6].

Increments in X and Y gradients are used to generate phase encoding in the transverse directions (Ox and Oy) by spin warping techniques. Axial velocities are computed by measuring the axial displacement of the tagged slice across the flow section as shown in Figure 3 [6].

The fid (free induction decay) transient signal received from the radio-frequency (RF) coil (200 MHz) was recorded using a Bruker MSL spectrometer. The static magnetic field was provided in the flow direction by a 4.7 Tesla solenoid magnet. The time of flight was about 30.7 ms. A 6 lobe sinc RF pulse of 3 ms duration in presence of axial magnetic gradients of 32 mT/m was used for cross-sectional slice selection of about 3 mm. Delay time between the echoes was set to 600 ms (3* T_1), and the cross-sectional spatial resolution was about of 32*32 pixels. Improved spatial cross sectional resolution (64x64) have also been performed. One to four repetitions were averaged to improve signal to noise ratios.

Axial velocities are determined by computing the first moments of the signal [2, 3, 4]. If $I(x,y,z)$ denotes the spin density, representing the fi-

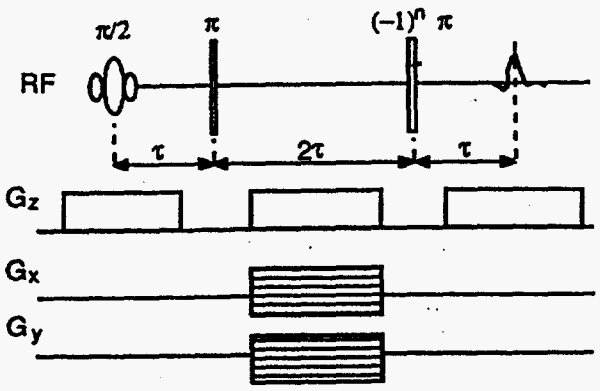

Figure 2: Time-of-flight spin-echo Flow Imaging NMR Pulse Sequence

Figure 3: Time-of-Flight Imaging Concepts: At time t=0, a slice of fluid is magnetized with a $\pi/2$ RF pulse (described above). The slice deforms due to the flow and is later imaged.

nal configuration of tagged spins after they have propagated along the flow direction z, the axial velocity is given by :

$$v(x,y) = \frac{1}{T_e} \frac{\int zI(x,y,z)dz}{\int I(x,y,z)dz} \tag{4}$$

where the echo time T_e is equal to 4 τ (See Figure 2).

Results and Discussion

The slurry was composed of 131 μm diameter PMMA (Polymethyl metacrylate) solid particles of density $\rho_s = 1.19$ g/cm^3 suspended in a low molecular weight polyether Newtonian oil (UCON Oil, 75-H-90,000) of 48 Poise viscosity and 1.10 g/cm^3 density, and in a mixture of water and sodium iodide to ensure neutrally buoyant conditions. A standard deviation of 51 μm for the particle distribution was measured using an electrical resistance technique. The solids loading of the slurry was varied from 21 % to 52 % and respectively pumped into 25 mm and 15 mm diameter pipes using a progressing cavity pump. Axial velocity surfaces of the fluid carrier across the pipe cross-section are presented in Figures 4 and 5 for the cases of 21 % and 52 % solids loadings. The mean carrier flow velocities are respectively 23 cm/s and 14.7 cm/s. Note that the NMR technique measures the instertitial fluid velocity only and not the superficial fluid velocity. Comparison of the model predictions and the experimental data is shown in Figure 6, where the experimental profiles are shown for two orthogonal cross-section directions. As can be seen, the flow is highly symmetrical and the model developed in this study predicts the blunted velocity profile characteristic of a neutrally buoyant suspension non-Newtonian slurry flow at high solids loading. Computations indicate that there is virtually no slip between liquid and solids phases and that the computed void fraction is basically constant across the pipe section. The latter observation was confirmed by measuring the liquid volume fraction by a NMR flow compensated technique which revealed an uniform liquid volume fraction across the pipe section.

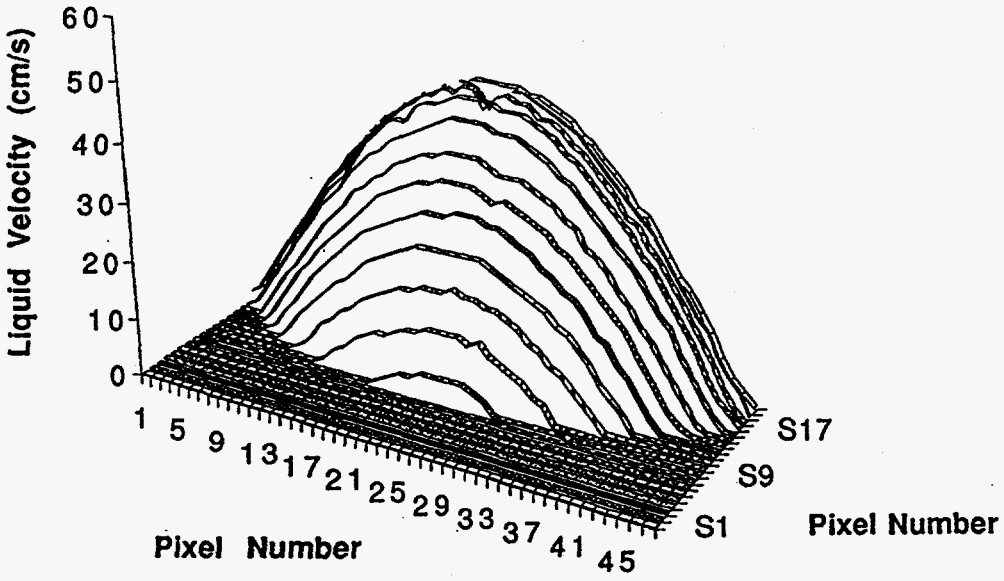

Figure 4: Axial Velocity Distribution Measured by NMR TOF technique (64x64 pixel resolution) for a 21 % solids laden slurry flow. Only half the distribution is presented for clarity

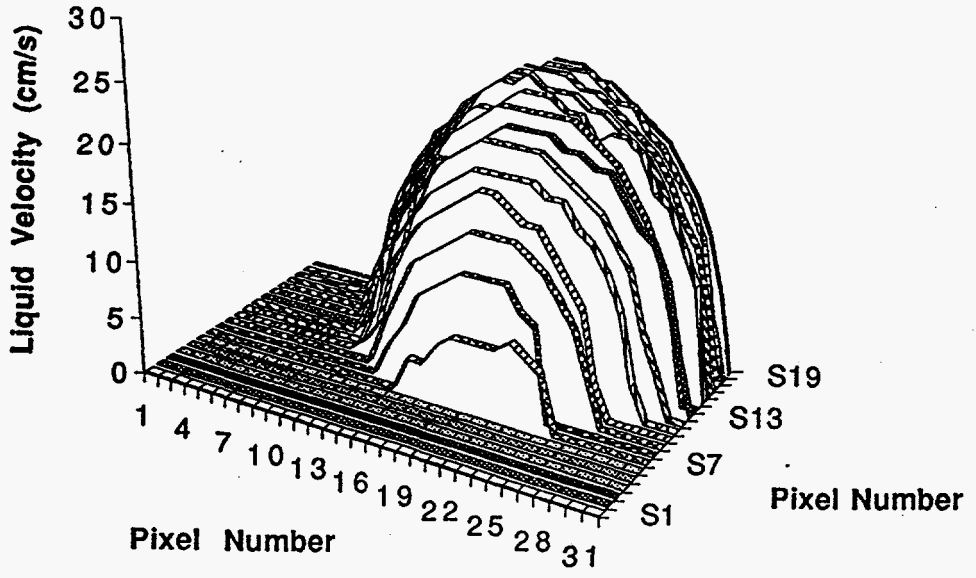

Figure 5: Axial Velocity Distribution Measured by NMR TOF technique (32x32 pixel resolution) for a 52 % solids laden slurry flow. Only half the distribution is presented for clarity

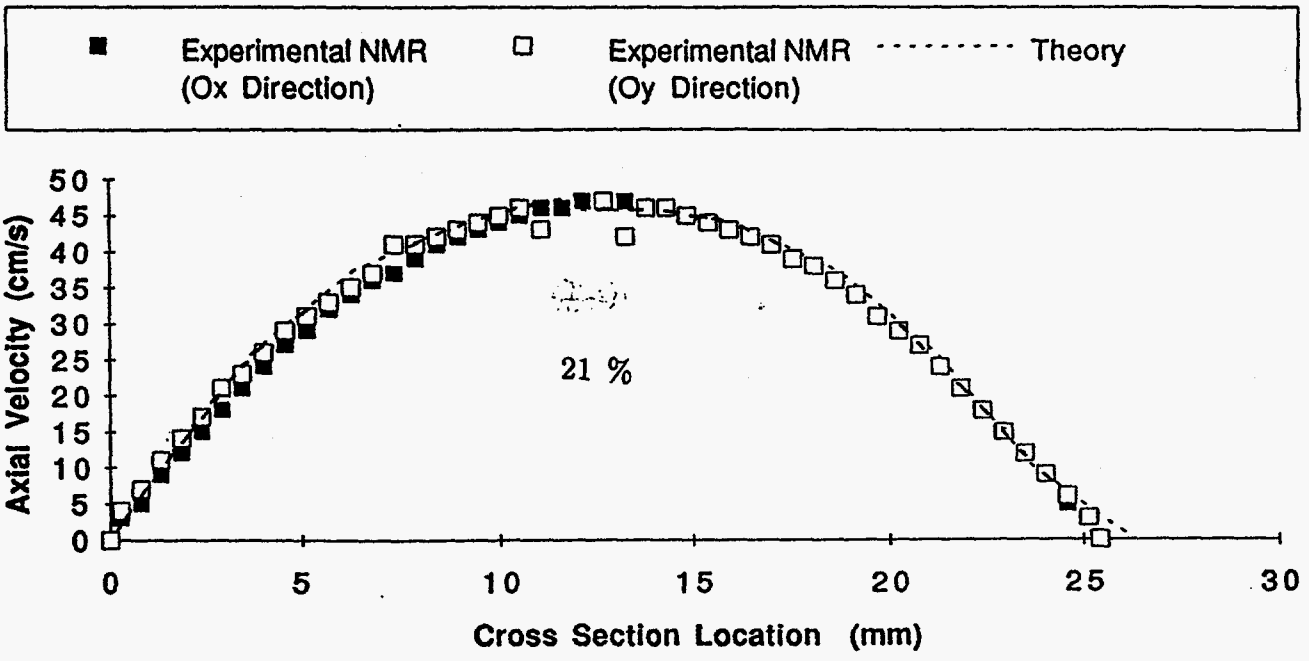

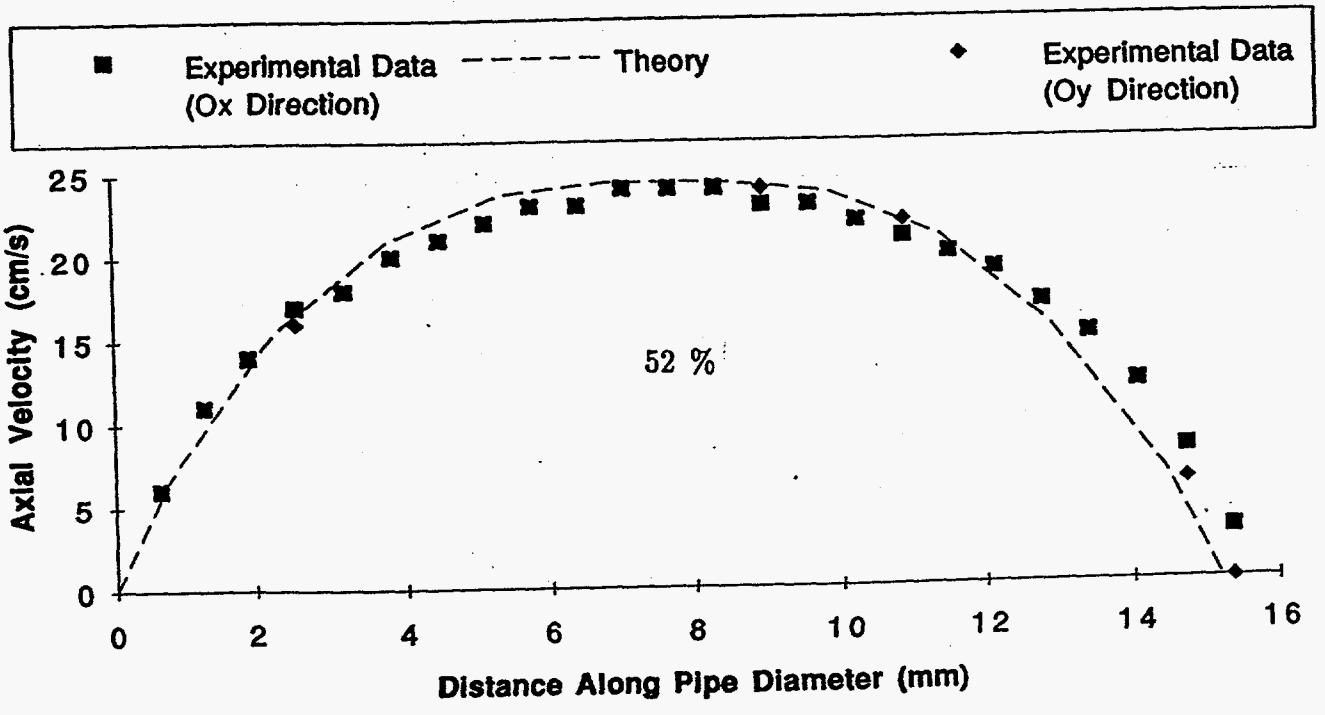

Figure 6: Comparison of Predicted and Experimentally Measured Axial Liquid Velocity for a 21 % and 52% solids suspensions.

Model Limitations and Future Work

Phenomenological constitutive equations for the slurry viscosity have been assumed in this model. It would be desirable to understand why the presence of particle, even at small concentrations, increases the slurry viscosity and why shear thinning occurs. To this date, these questions remained unanswered. It would also be important to experimentally measure the solids velocity especially near the pipe wall to ascertain the validity of velocity boundary conditions [19]. In addition, several carefully engineered NMR experiments await to be designed to measure forces that become important at high slip, such as Basset, lift, Magnus and added mass forces. There lies challenging research topics which need to be addressed and resolved if satisfactory understanding of such flow is to be provided.

Acknowledgment

This work was supported by the U. S. Department of Energy under the contract W-31-109-Eng-38.

Nomenclature

d_p	Particle diameter, m
$K(\epsilon_s)$	Slurry Consistency Index
$n(\epsilon_s)$	Slurry Power Law Index
$I(x,y,z)$	Proton Density, m^{-3}
G	Solids elastic modulus, Pa
G_x, G_y, G_z	Magnetic Field Gradients, T/m
g	Acceleration due to gravity, m/s^2
P	Pressure, Pa
T_1	Proton Longitudinal Relaxation Time, s
v_l	Liquid Velocity, m/s
v_s	Solids Velocity, m/s
v_{mix}	Mixture Velocity, m/s
Greek Letters	
β	Fluid-particle Friction Coefficient, $Kg/(m^3.s)$

ϵ_l	Liquid Phase Volume Fraction
ϵ_s	Solids Phase Volume Fraction
μ_l	Liquid Viscosity , kg/m/s
$\dot{\gamma}$	Shear rate, Hz
ρ	Density Kg/m^3
ϕ_s	Particle Sphericity
τ	Time Lag Between the RF $\pi/2$ Selective Pulse and the Hard π Pulse, s
τ_c	Compaction Solids Stress, Pa
τ_l	Liquid stresses , Pa
τ_s	Solids stresses, Pa
Operator	
$\nabla.$	Divergence
∇	Gradient

References

[1] P. D. Majors, R. C. Gilver, and E. Fukushima. Velocity and concentration measurements in multiphase flows by NMR. *J. Magn. Reson.*, 855:235–242, (1989).

[2] A. Caprihan and E. Fukushima. Flow measurement by NMR. *Phys. Rep.*, 198:195–235, (1990).

[3] S. A. Altobelli, A. Caprihan, and E. Fukushima. *NMR Flow Studies by Phase Methods.* San Francisco Press, San Francisco, 1990.

[4] S.A. Altobelli, R. C. Gilver, and E. Fukushima. Velocity and concentration measurements of suspensions by NMR Imaging. *J. Rheology*, 35(5):721–734, (1991).

[5] S. W. Sinton, J. H. Iwamiya, and A. W. Chow. NMR imaging of industrial flow processes. *Mat. Res. Soc. Symp. Proc.*, 217:73–78, (1991).

[6] S. W. Sinton and A. W. Chow. NMR flow imaging of fluids and solid suspensions in Poiseuille flows. *J. Rheology*, 35(5):735–772, (1991).

[7] Kose K., K. Satoh, T. Inouye, and H. Yasuoka. NMR flow imaging. *J. Phys. Soc. Jpn*, 54:81–92, (1985).

[8] Gidaspow D. Hydrodynamics of fluidization and heat transfer: supercomputer modeling. *Applied Mechanics Review*, 39(1):1–23, 1986.

[9] Bouillard J.X., R.W. Lyczkowski, and D. Gidaspow. Porosity distributions in a fluidized-bed with an immersed obstacle. *A.I.Ch.E. Journal*, 35(6), 1989.

[10] Bouillard J.X., R.W. Lyczkowski, S. Folga, D. Gidaspow, and G.F. Berry. Hydrodynamics of erosion of heat exchanger tubes in fluidized bed combustors. *Can. J. Chem. Eng.*, 67:908–922, 1989.

[11] J. X. Bouillard and D. Gidaspow. On the origin of bubbles and Geldart's classification. *J. Powder Technology*, 68:13–22, (1991).

[12] R. W. Lyczkowski and C. S. Wang. Hydrodynamic modeling and analysis of two-phase non-newtonian coal/water slurries. *J. Powder Technology*, 69:285–294, (1992).

[13] A. B. Basset. *Treatise on Hydrodynamics.* Deighton Bell, (1888).

[14] P. G. Saffman. The lift on a small sphere in slow shear flow. *J. Fluid Mech.*, 22:385–400, 1965.

[15] P. G. Saffman. Corrigendum. *J. Fluid Mech.*, 31:624, 1968.

[16] W. M. Swanson. The Magnus effect: a summary of investigation to date. *J. Basic Engng*, (1961).

[17] D. A. Drew and R. T. Lahey. The analysis of virtual mass effects in two-phase flow. *Int. J. Multiphase Flow*, 5, (1979).

[18] D. A. Drew, L. Cheng, and R. T. Lahey. The virtual mass and lift force on a sphere in rotating and straining inviscid flow. *Int. J. Multiphase Flow*, 13, (1987).

[19] S. L. Passman and D. A. Drew. An exact solution for shearing flow of muticomponent mixtures. *Chem. Eng. Sci.*, 46:2331–2338, (1991).